Donor-Acceptor Covalent Organic Framework Hollow Submicrospheres with Hierarchical Pore Structure for Visible-Light-Driven H_2 Evolution

Haiping Yu, [a,b] *Jianze Zhang,* [a,c] *Xiaorong Yan,* [d] *Chuanguang Wu,* [d] *Xiaoran Zhu,* [a,b] *Bowen Li,* [a,c] *Tengfei Li,* [a,c] *Qiuquan Guo,* [e,f] *Jiefeng Gao,* [g] *Mingjun Hu*[*,d] *and Jun Yang*[*a,b,e]

[a] Beijing Institute of Nanoenergy & Nanosystems, Chinese Academy of Sciences, Beijing, 101400, China.

[b] School of Nanoscience and Technology, University of Chinese Academy of Sciences, Beijing, 100049, China.

[c] Center on Nanoenergy Research, School of Physical Science and Technology, Guangxi University, Nanning 530004, China.

[d] School of Materials Science and Engineering, Beihang University, Beijing 100191, China.

[e] Shenzhen Institute for Advanced Study, University of Electronic Science and Technology of China, Shenzhen, 518000, China.

[f] School of Electronic Communication Technology, Shenzhen Institute of Information Technology, Shenzhen 518172, China.

[g] School of Chemistry and Chemical Engineering, Yangzhou University, Yangzhou 225002, China.

[*] Corresponding author, E-mail: mingjunhu@buaa.edu.cn, yangjun@binn.cas.cn.

1. Materials and Methods

1.1. Materials

4,4'-(thiazolo[5,4-d]thiazole-2,5-diyl)dibenzaldehyde (TZTZ-2BA) was prepared with reference to the previously reported method. 1,4-Terephthalaldehyde, dithiooxamide, Chloroplatinic acid hexahydrate, ascorbic acid, hexafluorophosphate ($TBAPF_6$), Lanthanum oxide (4,4′,4″,4‴-(ethene-1,1,2,2-tetrayl)tetraaniline ($4PE\text{-}4NH_2$) and 4,4'-Biphenyldicarboxaldehyde were obtained from Macklin. Silver nitrate was purchased by Aladdin. All the solvents were purchased from Aladdin and used as received without further purification.

1.2. General methods

1H nuclear magnetic resonance (NMR) spectra were tested on a Bruker AVANCE III HD500 (Bruker, Germany). Solid-state 13C CP/MAS NMR spectra were recorded on an Agilent 600 DD2 spectrometer (Agilent, USA) at the resonance frequency of 150.72 MHz for 13C using the cross-polarization (CP), magic-angle spinning (MAS), and a high-power 1H decoupling. The powder samples were placed in a pencil-type zirconia rotor of 4.0 mm o.d. The spectra were obtained at a spinning speed of 10 kHz (4.2 μs 90° pulses), a 2 ms CP pulse, and a recycle delay of 3 s. The C signal of tetramethylsilane (TMS) at 0 ppm was used as the reference of 13C chemical shift. Powder X-ray diffraction (PXRD) were recorded on a PANalytical Empyrean (PANalytical, Holland) with Cu Kα radiation (λ = 1.5418Å). High resolution mass spectra (HRMS) were recorded with an Agilent 7250 & JEOL-JMS-T100LP AccuTOF (Agilent, USA & JEOL, Japan). Fourier transform infrared (FT-IR) spectra were performed on a Bruker VERTEX80v (Bruker, Germany). Ultraviolet-visible diffuse reflectance spectra (UV-Vis DRS) were recorded on a UV3600 (Shimadzu, Japan) at room temperature. Nitrogen physisorption analyses were evaluated by an Autosorb iQ (Quantachrome, USA) at 77 K. Steady-state photoluminescence (PL) emission spectra and time-resolved fluorescence lifetime decay spectra were performed with an FLS1000 (Edinburgh, UK). Thermogravimetric analyses (TGA) were recorded on a TG-DTA8122 (Rigaku, Japan). The scanning electron microscopy (SEM) characterizations were performed on a Gemini 300 (ZEISS, Germany). Transmission electron microscope (TEM) measurements were conducted using a JEM-F200 (JEOL, Japan). X-ray photoelectron spectroscopy (XPS) measurements were performed on a Scientific K-Alpha (Thermo, USA). Photoelectrochemical characterization was performed on a PARSTAT MC (Princeton Applied Research, USA). Transient surface photovoltage (TS-SPV) was performed on a CEL-TPV2000 (Beijing China Education Au-light Co., Ltd).

1.3 Electrochemical measurements

FTO conducting glasses were cleaned by sonication in ethanol for 30 min and then dried in a vacuum oven. The conductive side of the FTO glass was coated with COFs suspension solutions (2 mg/ml in isopropanol with a few drops of 5 wt% Nafion). After drying, fill the uncoated areas surrounding sample with epoxy resin. A Pt sheet was used as the counter electrode, an FTO glass as the working electrode and an Ag/AgCl electrode as the reference electrode to form a three-electrode test system. The electrolyte was 0.1 M Na_2SO_4 aqueous solution swept by N_2. The photocurrent

measurements were carried out on the electrochemical workstation of Princeton. The light source was supplied by a 300 W Xe-lamp with a 420 nm ultraviolet cut-off filter. Light-on and light-off were alternated every 50 seconds and cycled five times. Mott-Schottky (M-S) curves were measured at the frequency of 1000, 2000 and 3000 Hz with the perturbation signal of 5 mV, respectively. The EIS spectra were tested in the dark and in the light with a perturbation signal of 5 mV and a frequency range of 100 kHz to 0.01 Hz. In Cyclic voltammetry measurements, the reference electrode was replaced with Ag/Ag^+ electrode (corrected with Ferrocenium/ferrocene (Fc/Fc^+) as internal reference), with 0.1 M tetrabutylammonium hexafluorophosphate ($TBAPF_6$) in CH_3CN as the supporting electrolyte with a sweep rate of 20 mV/s.

1.4 Photocatalytic measurements

The 10 mg of COFs were placed in a reactor followed by the addition of the 10 ml of isopropanol, and then evenly dispersed by ultrasound. Subsequently, the solids were taken out by centrifugation after homogenization and transferred to a reactor with top-irradiation and connected to a closed gas system (CEL-PAEM-D8Pro, Beijing China Education Au-light Co., Ltd), and the co-catalyst and sacrificial reagent were also added. The reaction system was dosed at 50 ml. For ensuring complete removal of air, the suspension of the mixture was carefully evacuated several times, and followed by irradiation with a 300 W xenon lamp with a suitable filter for a period of time. The amounts of H_2 and O_2 were analyzed by gas chromatography (GC-2014, Shimadzu) with a 5 Å molecular sieve column with the Ar as the carrier gas and a thermal conductivity detector (TCD). After the photocatalytic reaction, the catalysts were washed and dried, and then collected for the next analytical characterization. In the photocatalytic hydrogen reduction test, we added 10 mg of samples (after ultrasonic dispersion) to 50 ml of water containing ascorbic acid as an electron sacrificial agent and Pt (3 wt%) as a co-catalyst under visible light ($\lambda > 420$ nm) irradiation with the reaction temperature of 6 °C. Other conditions were kept constant, and the effect of different mass fractions of Pt and different sacrificial reagents on the reaction results was investigated. The photocatalytic activity of O_2 production was tested under visible light ($\lambda > 420$ nm) irradiation in pure water with aqueous silver nitrate solution (0.01 M, 50 mL) as the electron acceptor. The apparent quantum efficiency (AQE) measurements were implemented under irradiation of 300 W Xe lamp with bandpass filters (420 ± 10 nm, 520 ± 10 nm), and the light intensities were 10 and 10.8 mW/cm^2, respectively. The experimental conditions are the same as those of photocatalytic hydrogen production. The light irradiation area was measured in $\pi \times 2.5 \times 2.5$ cm^2. The AQE is calculated by the following equation：

$$\eta_{AQY} = \frac{N_e}{N_p} \times 100\% = \frac{2 \times M \times N_A}{\frac{E_{total}}{E_{Photon}}} \times 100\% = \frac{2 \times M \times N_A}{\frac{S \times P \times t}{h \times \frac{c}{\lambda}}} \times 100\% = \frac{2 \times M \times N_A \times h \times c}{S \times P \times t \times \lambda} \times 100\%$$

where N_e is the amount of generated electrons, N_p is the incident photons, M is the amount of H_2 molecules (mol), N_A is Avogadro constant (6.022×10^{23} mol^{-1}), h is the Planck constant (6.626×10^{-34} J·s), c is the speed of light (3×10^8 m·s^{-1}), S is the irradiation area (cm^2), P is the intensity of irradiation light (W·cm^{-2}), t is the photoreaction time (s), λ is the wavelength of the monochromatic light (m).

1.5 Theoretical Calculations

The DFT calculations were performed using Gaussian16 for figuring out the electronic characteristics of the PETZ-COF and PEBP-COF.[1] For geometry optimization and frequency calculations, the PBE0 [2, 3] functional was adopted with the D3(BJ) empirical dispersion correction[4] and 6-311G(d) basis set.[5, 6] Visualization of the optimized geometrical structures and frontier molecular orbitals were displayed by VMD.[7] Meanwhile, we also calculated the free energy change (ΔG_{H^*}) in the photocatalytic H_2 evolution reaction, and the reference calculation formula is as follows: $\Delta G_{H^*} = \Delta E + \Delta E_{ZPE} + \Delta G_{0\to T} - eU$, where ΔE is the DFT electronic energy difference of each step, ΔE_{ZPE} and $\Delta G_{0\to T}$ are the correction of zero-point energy and the contribution of heating from 0K to room temperature to thermodynamic quantity, respectively, which are obtained by vibration analysis. The U is a potential bias due to a light-induced electrons/holes in contrast to the NHE.[8, 9] The hydrogen evolution rate (HER) process is a two-electron transfer reaction divided into two steps, the first being a proton/electron transfer step and the second being a hydrogen release step.

$$* + H^+ + e^- \rightarrow H^*$$

$$H^* + H^+ + e^- \rightarrow * + H_2\,(g)$$

Where * represents the adsorption site and H^* denotes the adsorbed H^+ ions.[9-11]

2. Synthetic Procedures

2.1. Synthesis of 4,4'-(thiazolo[5,4-d]thiazole-2,5-diyl)dibenzaldehyde (TZTZ-2BA)

The synthetic method was based on the previously reported work[12]. 1H NMR (400 MHz, $CDCl_3$): δ 10.12 (s, 2H), 8.23 (d, J = 8.2 Hz, 4H), 8.04 (d, J = 8.3 Hz, 4H). HR-MS: m/z calcd for $C_{18}H_{10}N_2O_2S_2$ $[M + H]^+$: 351.02, found: 350.84.

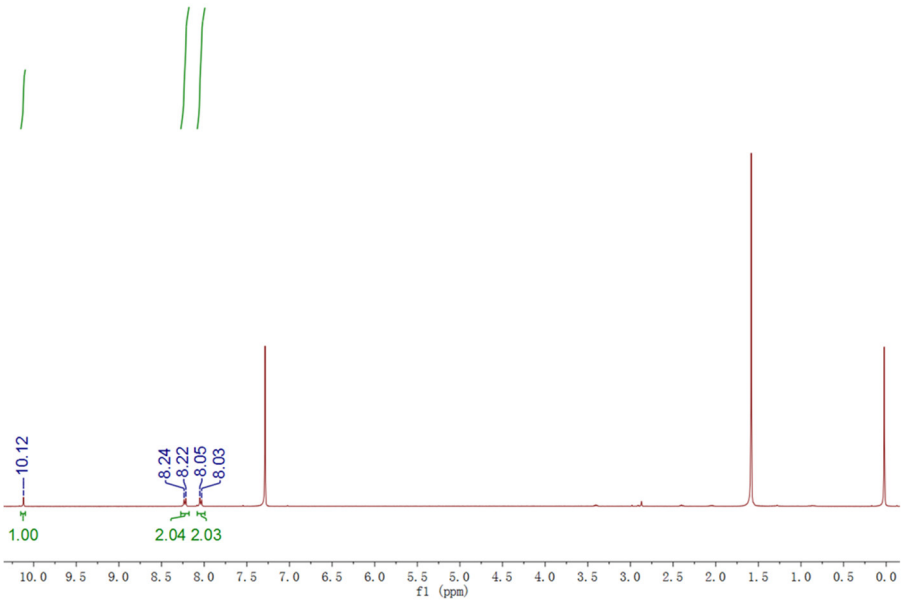

Figure S1. 1H NMR (CDCl3) of TZTZ-2BA.

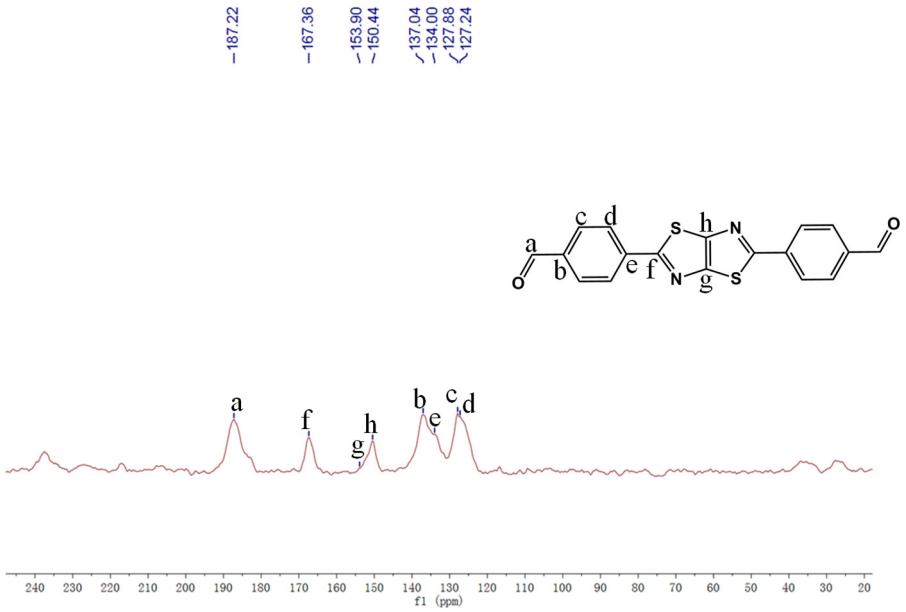

Figure S2. Solid-state ^{13}C CP-MAS NMR of TZTZ-2BA.

2.2. Synthesis of PETZ-COF

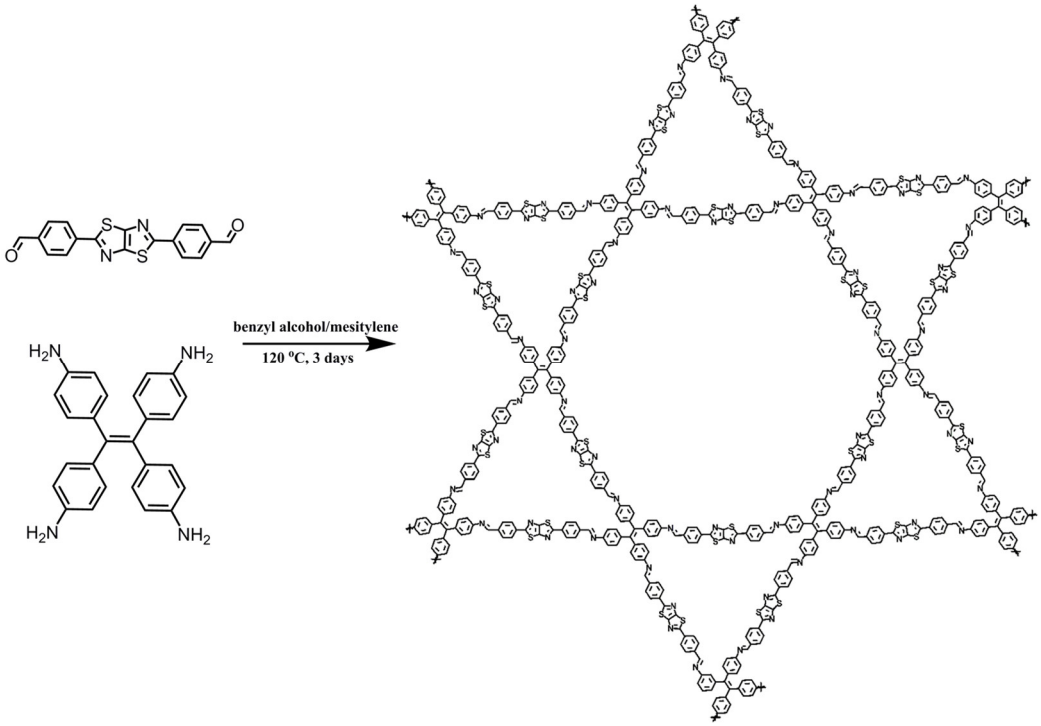

Figure S3. Scheme of the synthesis of PETZ-COF

2.3. Synthesis of PEBP-COF

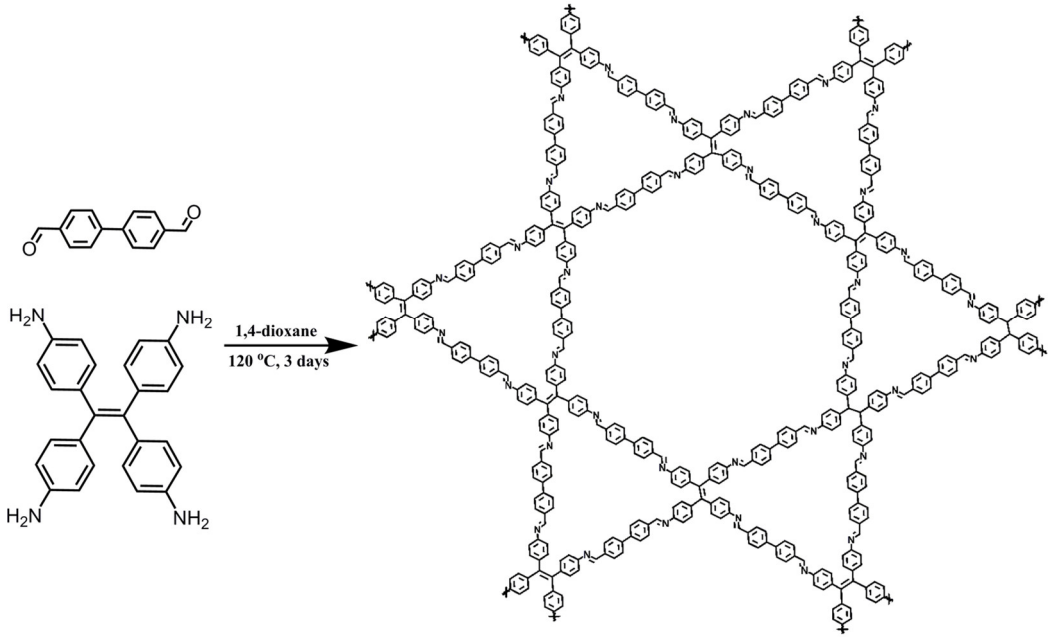

Figure S4. Scheme of the synthesis of PEBP-COF

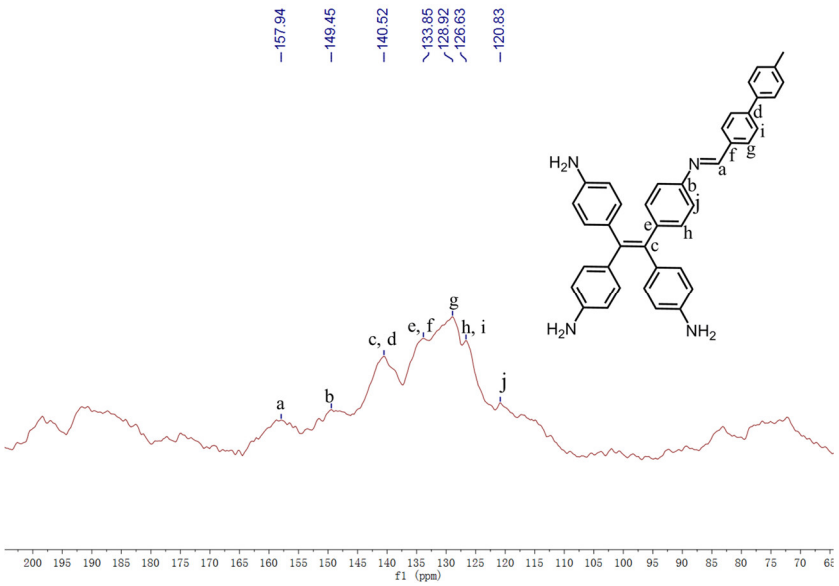

Figure S5. Solid-state 13C CP-MAS NMR of PEBP-COF.

3. Structural Simulation

Pawley refinements of the PXRD patterns were done in the Reflex module, and the results show that the PETZ-COF and PEBP-COF conforms to the *P*6 space group and AA stacking mode. The integrated intensities were extracted using Pseudo Voigt profile. The unit cell parameters a, b, c, FWHM parameters U, V, W, profile parameters NA, NB, and zero point were refined. The background was refined with 20th order polynomial. The theoretical models of PETZ-COF were optimized via the Forcite module. The corrected atomic coordinates of PETZ-COF are placed in table S1.

Table S1. Crystal system, space group, and unit cell parameters of PETZ-COF.

PETZ-COF *P*6 a=b=56.46 Å, c=4.4 Å $\alpha=\beta=90°$, $\gamma=120°$			
Atom Name	x	y	z
S1	0.28558	0.50781	0.9249
S2	0.20117	0.45136	0.90895
N3	0.37976	0.45441	0.44765
N4	0.25006	0.45557	0.82129
N5	0.10785	0.505	0.40206
N6	0.23694	0.50397	0.8319
C7	0.34583	0.48193	0.5332

C8	0.33563	0.45166	0.47673
C9	0.30695	0.43842	0.33994
C10	0.28754	0.44086	0.56191
C11	0.3269	0.48511	0.75579
C12	0.44171	0.44843	0.24944
C13	0.41705	0.44507	0.4263
C14	0.40039	0.45477	0.24602
C15	0.41895	0.48395	0.13087
C16	0.44279	0.4859	-0.05353
C17	0.48784	0.48441	-0.01383
C18	0.46027	0.47803	0.14318
C19	0.29718	0.47095	0.64073
C20	0.35547	0.44806	0.27226
C21	0.27899	0.47296	0.88671
C22	0.14209	0.47839	0.51334
C23	0.1524	0.50879	0.46322
C24	0.18158	0.52252	0.34101
C25	0.20026	0.51947	0.56952
C26	0.16034	0.47479	0.74211
C27	0.04572	0.50702	0.34684
C28	0.07697	0.52289	0.34085
C29	0.08929	0.50708	0.18815
C30	0.06775	0.47839	0.08201
C31	0.04501	0.47875	-0.10463

C32	0.0343	0.49701	0.03122
C33	0.19031	0.4892	0.63771
C34	0.13348	0.51282	0.24711
C35	0.25049	0.49481	1.04274
C36	0.23602	0.46387	1.03506
C37	0.20782	0.48627	0.88607
H38	0.33472	0.5072	0.79392
H39	0.29932	0.41644	0.29341
H40	0.26685	0.43115	0.45689
H41	0.45313	0.44196	0.39725
H42	0.40387	0.42328	0.49197
H43	0.40697	0.49035	-0.0125
H44	0.45442	0.50685	-0.14321
H45	0.34583	0.42657	0.19034
H46	0.12085	0.46802	0.60246
H47	0.18939	0.54462	0.30123
H48	0.22125	0.52954	0.4738
H49	0.03754	0.51868	0.45939
H50	0.08472	0.54297	0.22728
H51	0.07758	0.46905	-0.05346
H52	0.02894	0.45755	-0.15277
H53	0.14679	0.45258	0.81496
H54	0.1424	0.53522	0.18341
H55	0.3667	0.49908	0.45546

Table S2. Crystal system, space group, and unit cell parameters of PEBP-COF.

PEBP-COF *P*6
a=b=45.82 Å, c=4.63 Å
α=β=90°, γ=120°

Atom Name	x	y	z
C1	0.48521	0.48505	0.33715
C2	0.45335	0.48445	0.355
C3	0.42769	0.46467	0.16316
C4	0.39915	0.46706	0.15615
C5	0.39606	0.48933	0.34103
C6	0.42109	0.50817	0.543
C7	0.44924	0.50514	0.55084
H8	0.46992	0.51998	0.69898
C9	0.48231	0.45204	0.32092
C10	0.45519	0.42493	0.45709
C11	0.45143	0.39338	0.45176
C12	0.4753	0.38829	0.312
C13	0.50166	0.41477	0.16269
C14	0.50499	0.44603	0.16743
N15	0.36849	0.49322	0.32582
C16	0.3395	0.46724	0.3005
C17	0.31043	0.4709	0.2792
C18	0.28066	0.44644	0.4034
C19	0.25437	0.45239	0.43515
C20	0.25751	0.48218	0.33035
C21	0.28714	0.5062	0.19924

C22	0.31356	0.50057	0.17094
N23	0.472	0.35705	0.31889
C24	0.49815	0.35426	0.3459
C25	0.49535	0.32178	0.33491
C26	0.52083	0.3169	0.44309
C27	0.51682	0.28515	0.44233
C28	0.48725	0.25838	0.33663
C29	0.46179	0.26334	0.22826
C30	0.46596	0.29494	0.22484
H31	0.43128	0.44846	0.01124
H32	0.37963	0.45345	-0.00609
H33	0.41739	0.52476	0.68887
H34	0.43705	0.42933	0.57361
H35	0.43088	0.37226	0.56419
H36	0.51888	0.40979	0.03771
H37	0.5259	0.46676	0.05485
H38	0.33591	0.44164	0.32268
H39	0.27941	0.42384	0.49309
H40	0.23121	0.43439	0.54447
H41	0.28823	0.52871	0.10931
H42	0.33725	0.51868	0.06936
H43	0.52314	0.37636	0.39103
H44	0.54333	0.33819	0.53486
H45	0.53608	0.28037	0.53011

H46	0.43899	0.24176	0.14486
H47	0.44693	0.30037	0.14256

2. Supporting figures and tables.

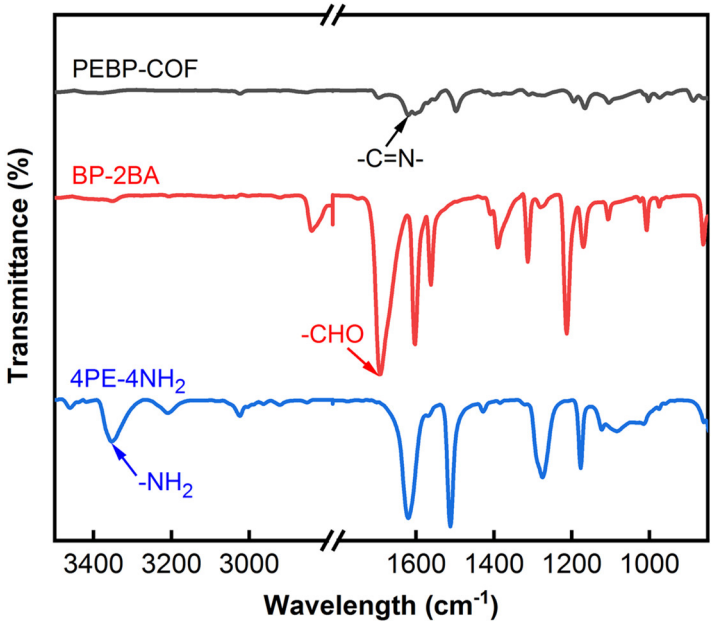

Figure S6. FT-IR spectra of PEBP-COF, 4PE-4NH_2, BP-2BA.

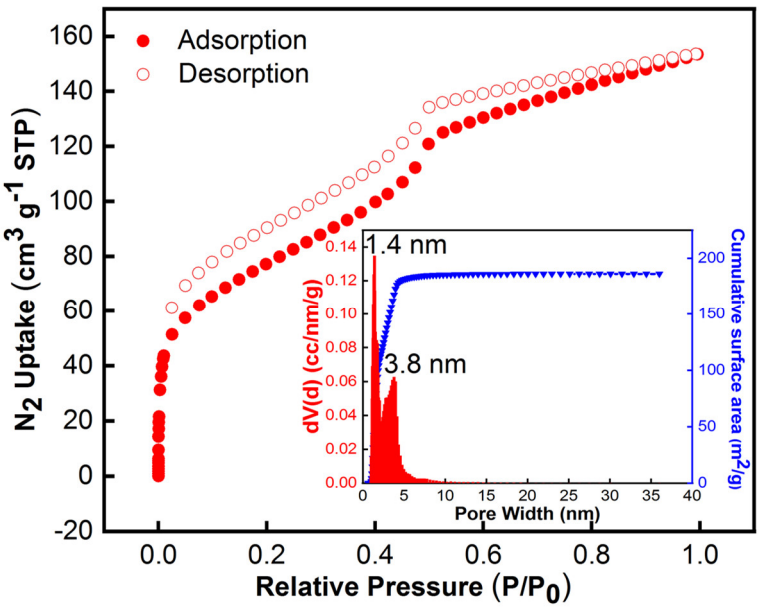

Figure S7. Nitrogen adsorption isotherm of PEBP-COF at 77 K and the inset shows the derived pore size distribution.

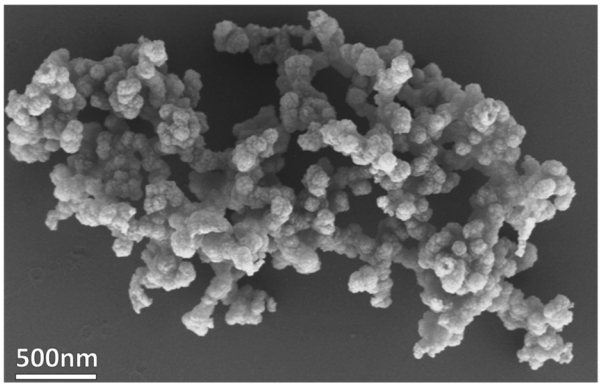

Figure S8. SEM image of PETZ-COF.

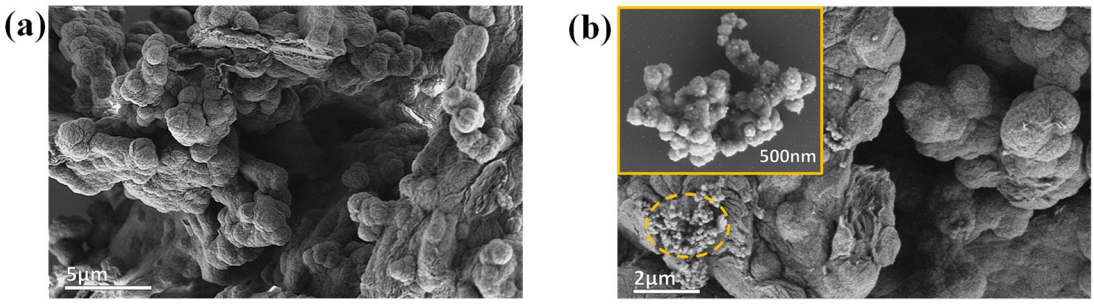

Figure S9. (a, b) SEM images of PEBP-COF.

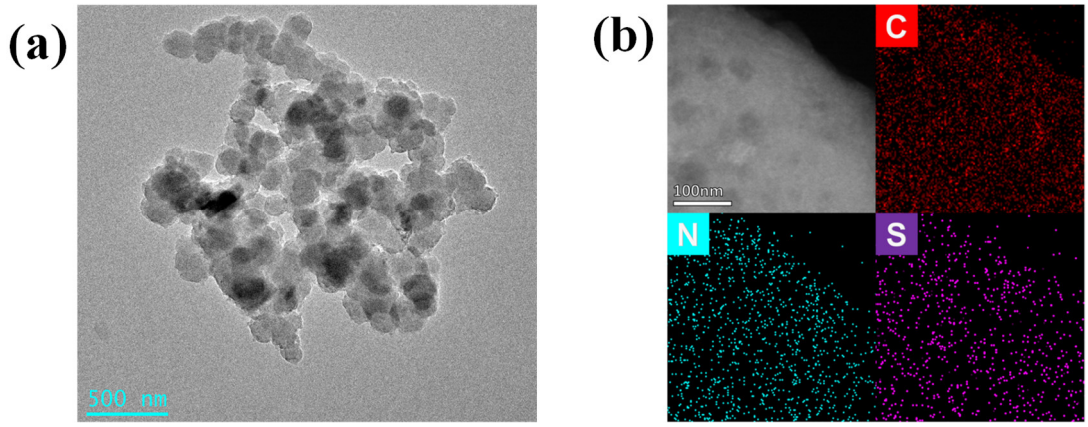

Figure S10. (a) TEM image of PETZ-COF. (b) EDX spectrum of PETZ-COF.

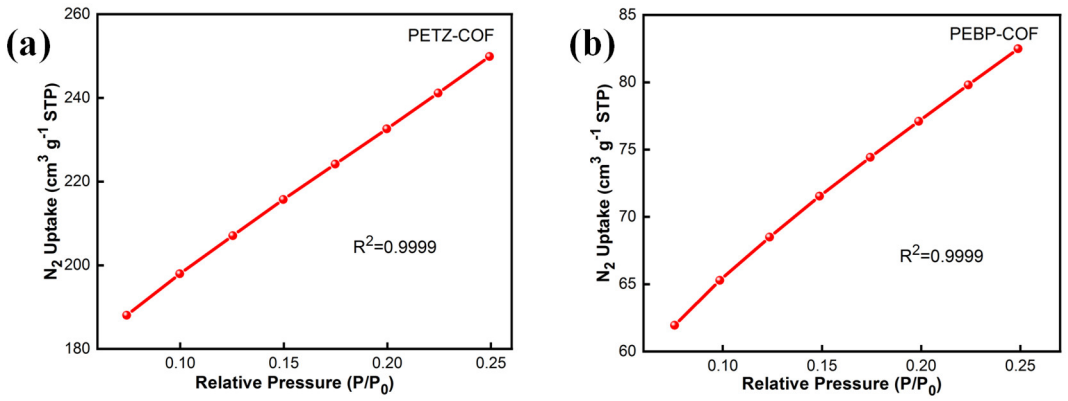

Figure S11. BET plot of (a) PETZ-COF and (b) PEBP-COF calculated from N2 adsorption isotherm at 77 K.

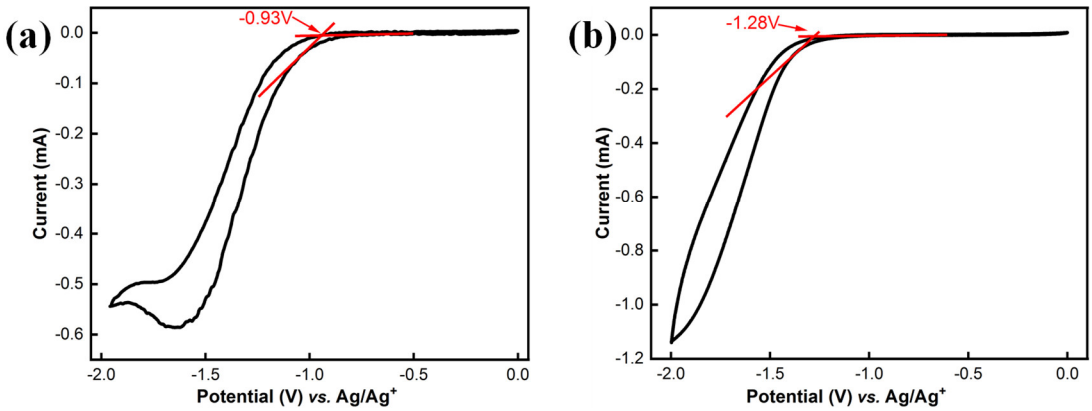

Figure S12. Cyclic voltammograms (C-V) of (a) PETZ-COF, (b) PEBP-COF.

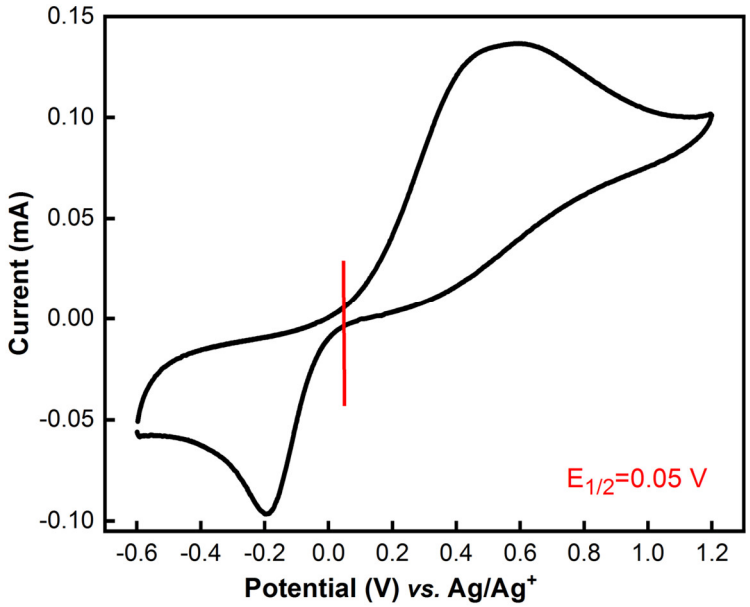

Figure S13. Cyclic voltammogram of Fc/Fc^+.

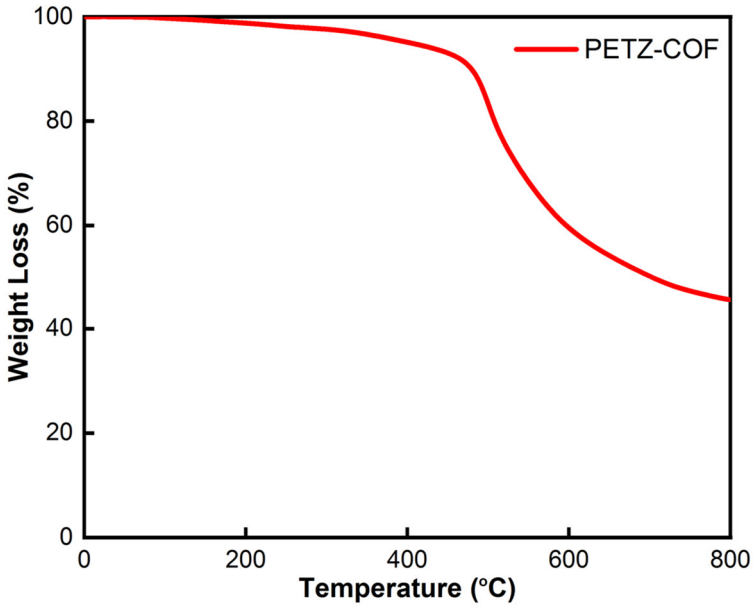

Figure S14. TGA trace of PETZ-COF under N_2 atmosphere.

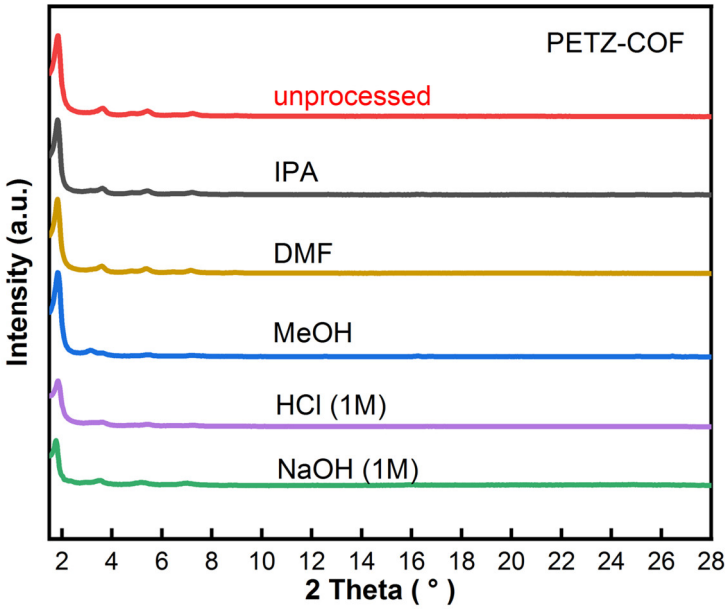

Figure S15. PXRD pattern of PETZ-COF soaked in different solutions for 24h.

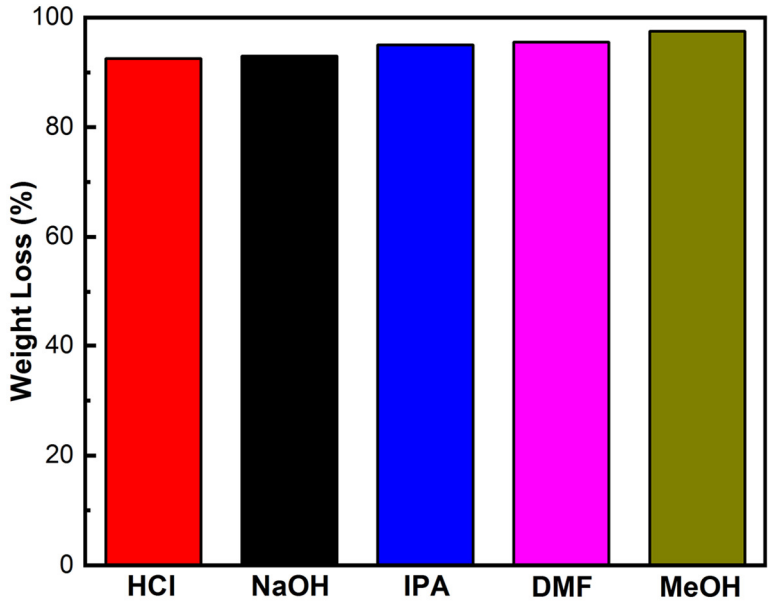

Figure S16. Residual weight percentage of PETZ-COF after treatment in different solvents for 24 h.

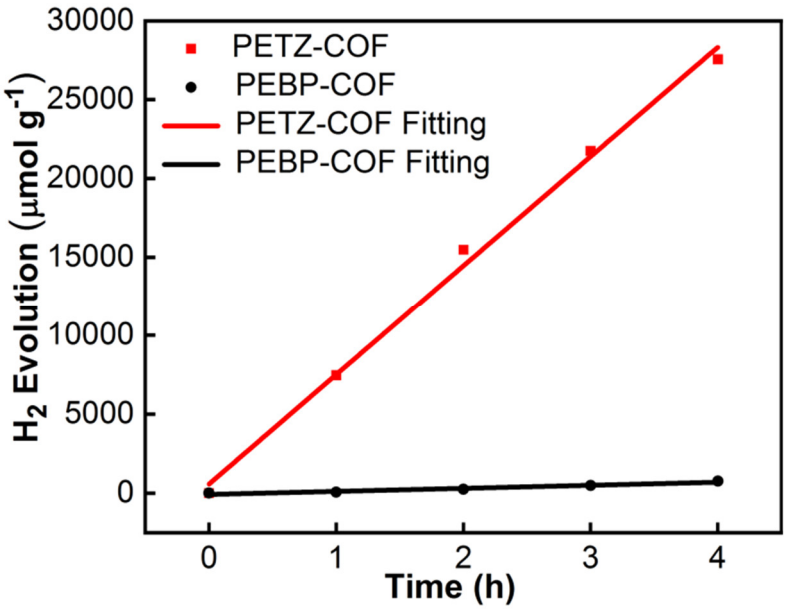

Figure S17. Hydrogen evolution rate of the PETZ-COF and PEBP-COF under visible light ($\lambda > 420$ nm).

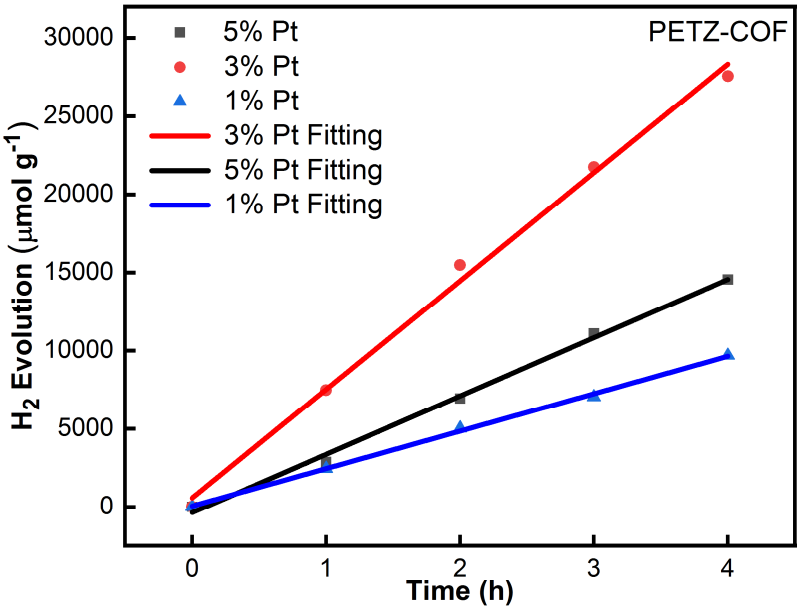

Figure S18. H_2 evolution rate of PETZ-COF with different Pt loading amounts under visible light ($\lambda > 420$ nm) illumination.

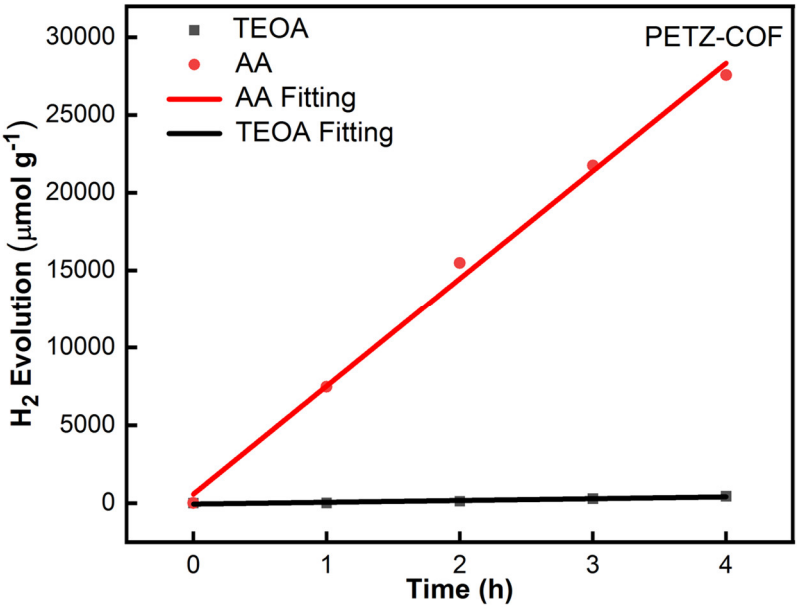

Figure S19. H_2 evolution rate of PETZ-COF with different sacrificial agents amount under visible light ($\lambda > 420$ nm) illumination.

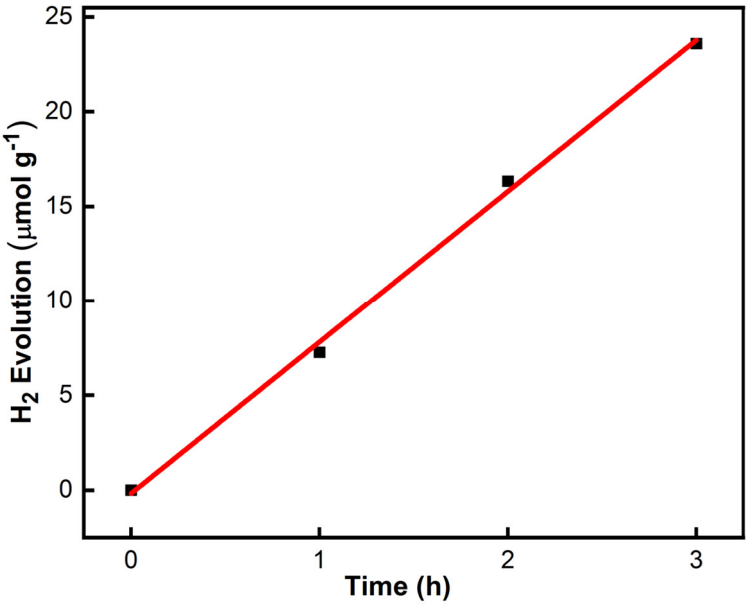

Figure S20. H_2 evolution rate of PETZ-COF without any sacrificial agents amount under visible light (λ > 420 nm) illumination.

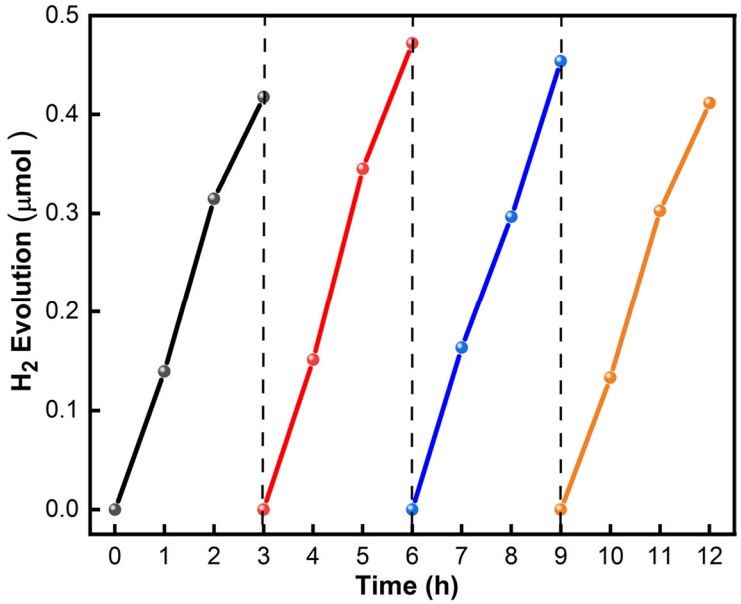

Figure S21. Cycling stability of H_2 evolution of PETZ-COF tested over 12 h with evacuation every 3 h under visible light irradiation (λ > 420 nm) without adding Pt cocatalyst.

The steady HER without significant decay can be observed during the continuous photocatalytic reaction (12 h) for PETZ-COF under visible light irradiation (λ > 420 nm) without adding Pt cocatalyst.

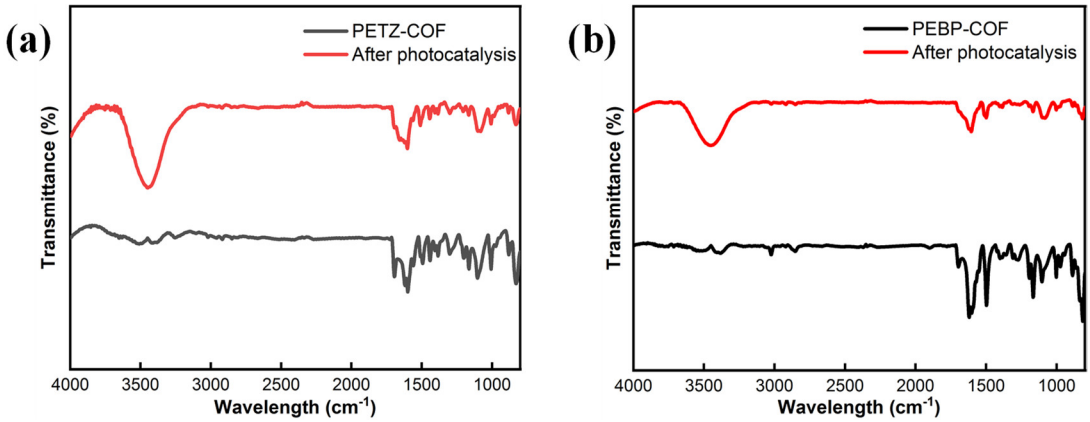

Figure S22. FT-IR spectra of (a) PETZ-COF and (b) PEBP-COF before and after of photocatalysis.

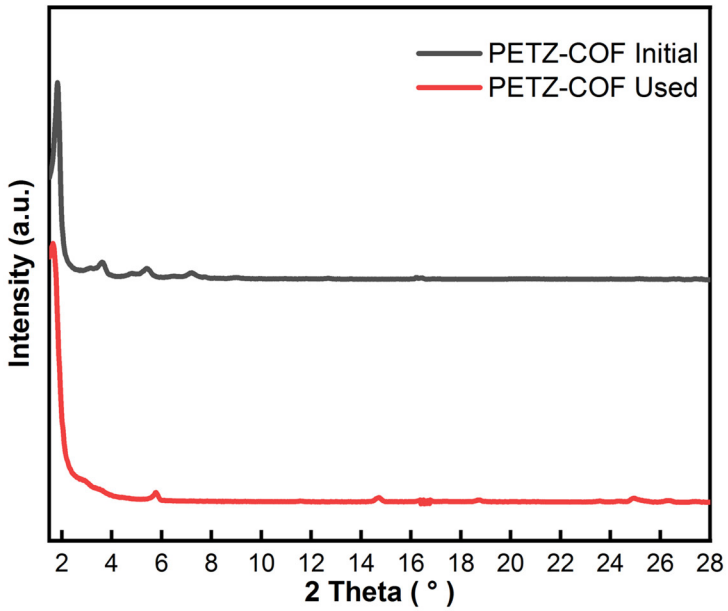

Figure S23. PXRD pattern of PETZ-COF before and after photocatalysis.

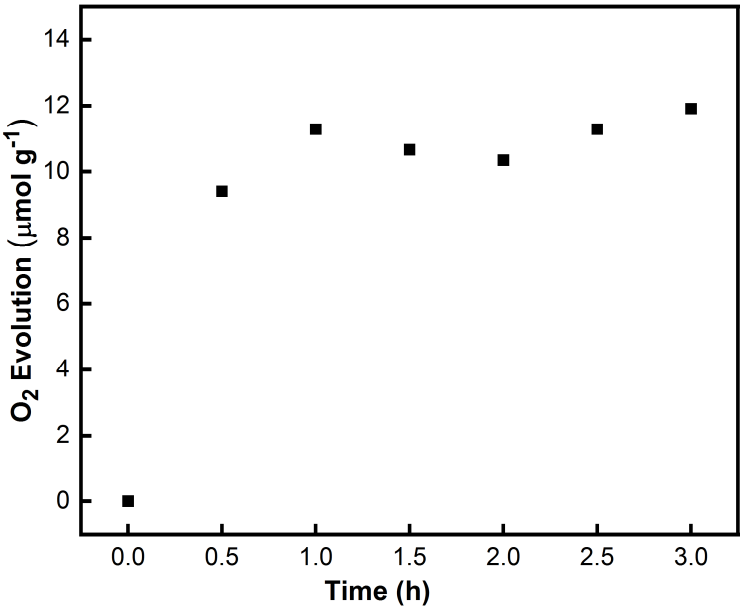

Figure S24. O_2 evolution rate of PETZ-COF in pure water with $AgNO_3$ as electron acceptor under visible light (λ > 420 nm) illumination.

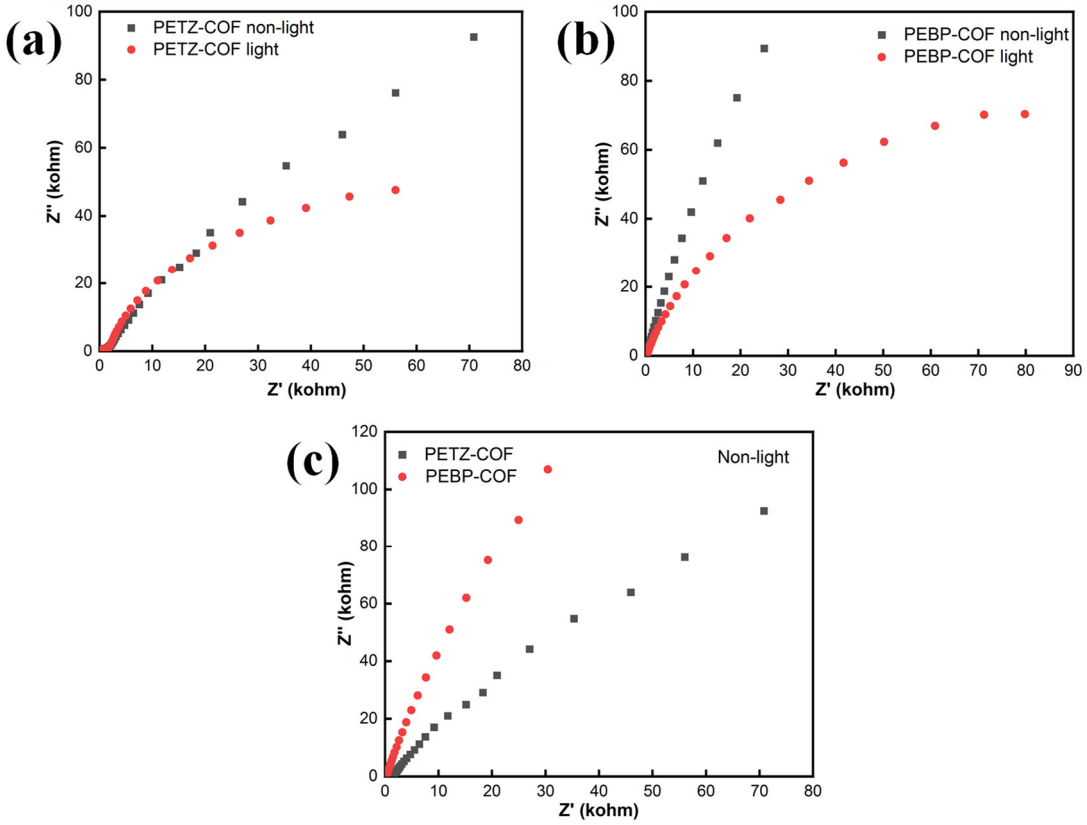

Figure S25. EIS Nyquist plots of (a) PETZ-COF under visible light (λ > 420 nm) and non-light illumination. (b) PEBP-COF under visible light (λ > 420 nm) and non-light illumination. (c) PETZ-COF and PEBP-COF under non-light illumination.

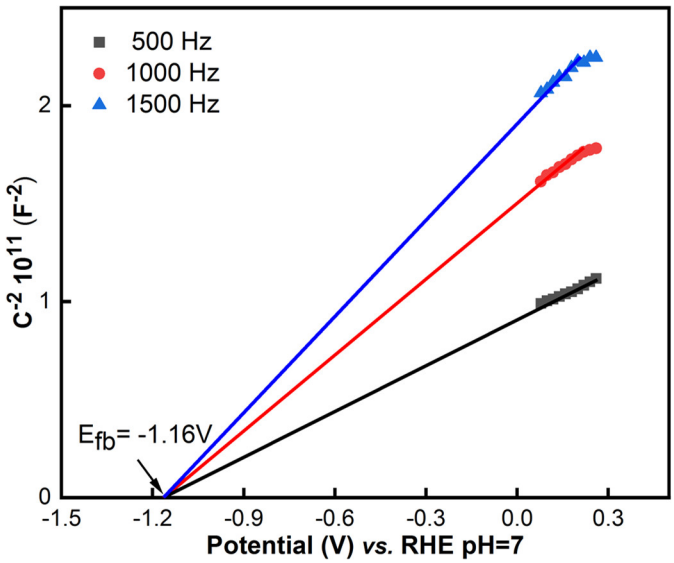

Figure S26. Mott-Schottky (M-S) plot of the PEBP-COF at 500, 1000, and 1500 Hz.

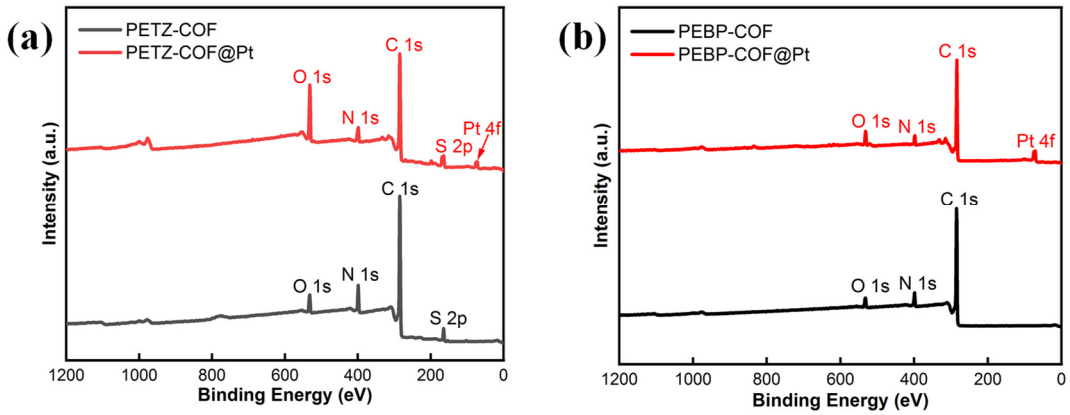

Figure S27. XPS survey spectra of (a) PETZ-COF and (b) PEBP-COF before and after photocatalysis.

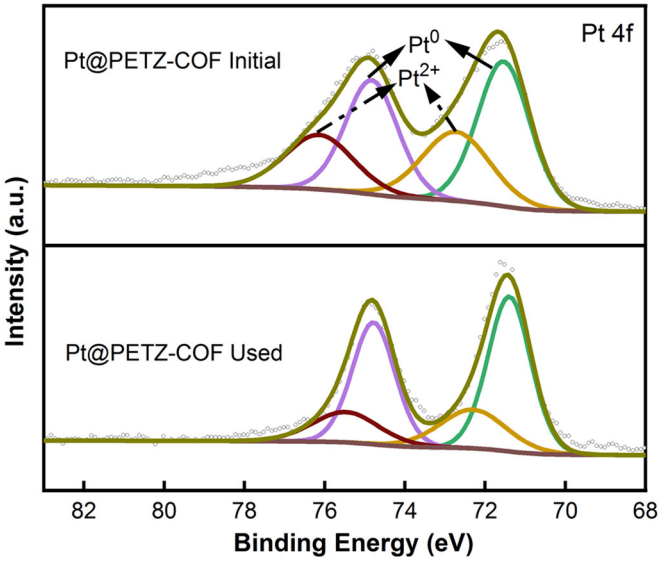

Figure S28. High-resolution Pt 4f XPS spectra of Pt@PETZ-COF before and after photocatalysis.

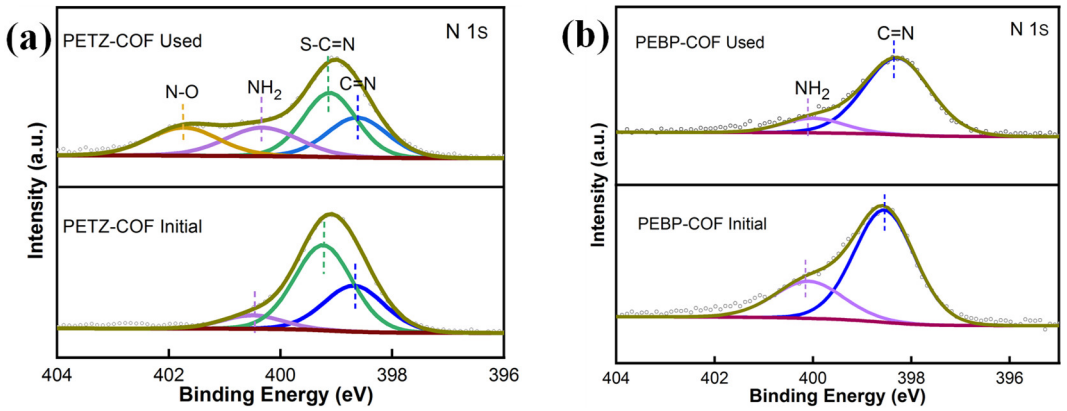

Figure S29. High-resolution N 1s XPS spectra of (a) PETZ-COF and (b) PEBP-COF before and after photocatalysis.

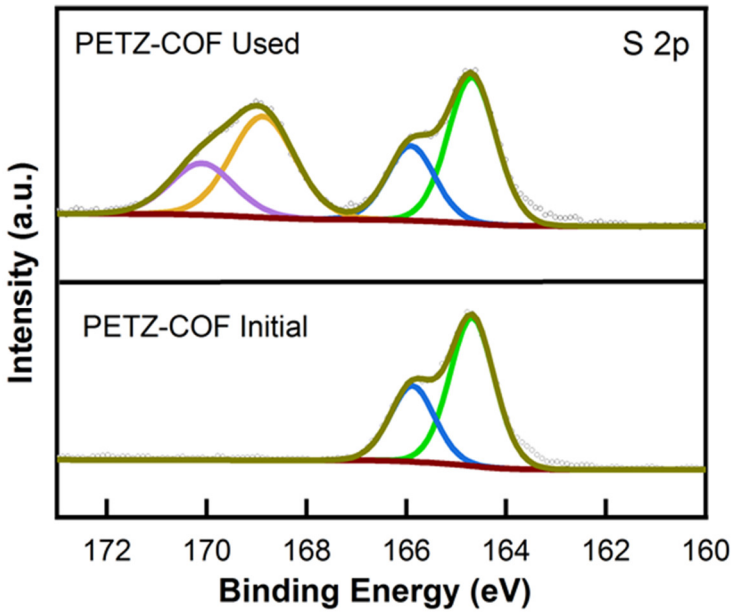

Figure S30. High-resolution S 2p XPS spectra of PETZ-COF before and after photocatalysis.

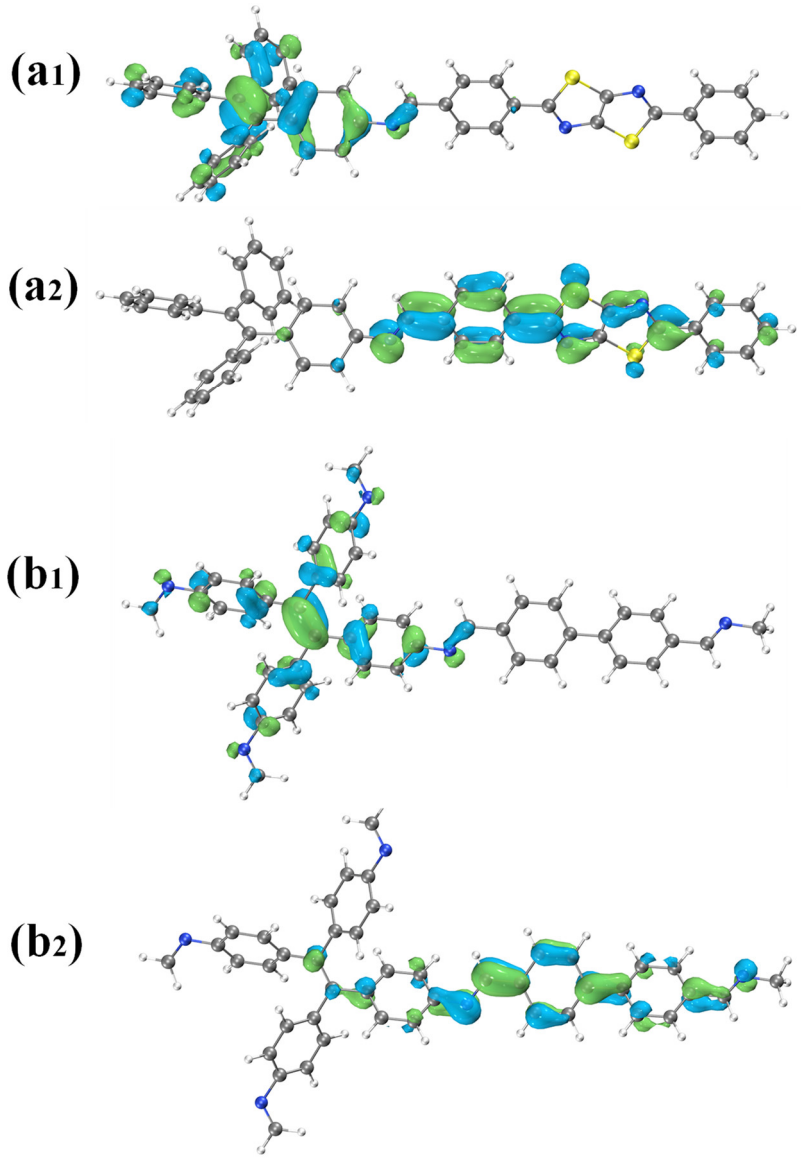

Figure S31. Optimized frontier orbitals by DFT simulation of (a1, b1) HOMO of PETZ-COF and PEBP-COF and (a2, b2) LUMO of PETZ-COF and PEBP-COF.

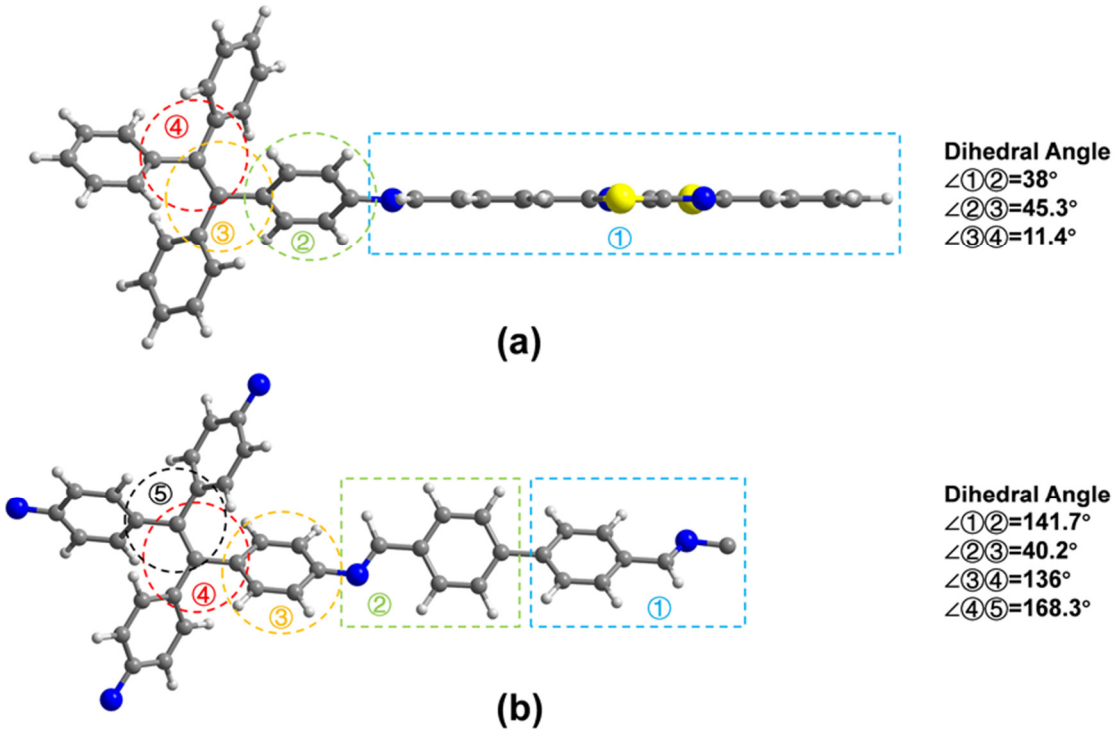

Figure S32. Dihedral angle of (a) PETZ-COF (b) PEBP-COF. Clockwise is the positive direction.

Table S3. Values of frontier orbitals by DFT simulation.

Sample	HOMO	LUMO
PETZ-COF	-5.603188 eV	-2.465770 eV
PEBP-COF	-5.475364 eV	-2.039926 eV

Table S4. Synthetic conditions that were screened for synthesizing PETZ-COF.

Entry	Solvent1 ml	Solvent2 ml	Catalyst ml	T/℃	Time/days	Crystallinity
1	Dioxane/3	Mesitylene/3	HOAc/6M,0.6	120	3	poor
2	DMF/3	Mesitylene/3	HOAc/6M,0.6	120	3	poor
3	Dioxane/3	o-DCB /3	HOAc/6M,0.6	120	3	poor
4	Dioxane/3	DMF/3	HOAc/6M,0.6	120	3	poor
5	n-BuOH/3	Dioxane/3	HOAc/6M,0.6	120	3	poor
6	Dioxane/3	Mesitylene/3	HOAc/6M,0.6	120	4	poor
7	o-DCB /4	n-BuOH/2	HOAc/6M,0.6	120	4	poor
8	Dioxane/5.1	Mesitylene/0.9	HOAc/0.2	120	3	poor
9	Dioxane/3	Mesitylene/3	HOAc/0.2	120	3	poor
10	Benzyl alcohol/0.9	Mesitylene/0.1	HOAc/0.1	120	3	fine
11	Benzyl alcohol /1.8	Mesitylene/0.2	HOAc/0.2	120	3	best
12	Benzyl alcohol /3.6	Mesitylene/0.4	HOAc/0.4	120	3	fine

Table S5. The outline of performances of PETZ-COF and other D-A COFs for Visible-Light-Driven H_2 Evolution and O_2 Evolution.

COFs	**HER ($\mu mol\ g^{-1}\ h^{-1}$)**	**AQE(%)**	**Conditions (HER)**	**Reference**
PETZ-COF	**7324.3**	**3.64 (520nm)**	**Pt (3 wt%)** **0.1 M AA** **λ>420 nm** **6 °C**	**This work**
PyTz-COF[12]	2072.4	----*	Pt(3 wt%) 0.1 M AA AM 1.5 --*	*Angew.Chem.Int. Ed.,**2021**,60,1869.*
BTH-1 BTH-2 BTH-3[13]	10500 1200 15100	1.925 (500nm) 0.241 (500nm) 1.256 (500nm)	Pt (8 wt%) 0.1 M AA λ>420 nm 5 °C	*Nat.Commun,**2022**,13,100.*
HBT-COF BT-COF[14]	680 3800	----*	Pt (3 wt%) 0.1 M AA λ>420 nm 5 °C	*ACS Appl. Mater. Interfaces **2021**,13, 27041.*
BtCOF150[15]	750	0.2 (420nm)	Pt (1 wt%) TEOA(10 vol %) λ>400 nm --*	*J.Am.Chem. Soc.**2020**,142, 9752.*
sp^2c-COF sp^2c-COF_{ERDN} sp^2c-CMP[11]	1,360 2,120 140	----* 0.48 (495nm) ----*	Pt (3 wt%) TEOA(10 vol %) λ>420 nm 12 °C	*Chem, **2019**, 5, 1632.*
NKCOF-108[9]	11600	2.96 (520nm)	Pt (5 wt%) 0.1 M AA λ>420 nm 5 °C	*ACS Catal. **2021**,11,2098.*
PMDA-COF DHTA-COF TPAL-COF[16]	435.6 56.2 6.8	----* ----* ----*	Pt (3 wt%) TEOA(10 vol %) λ>420 nm 4 °C	*J.Photochem.&Photobio.,A:Chem. **2021**,421,113546*
COFs-1 COFs-2 COFs-3 COFs-4[17]	1033.38 1443.98 2789.46 1274.13	----* ----* ----* ----*	Pt (1 wt%) TEOA(10 vol %) λ>420 nm --*	*ACS Appl. Energy Mater. **2021**,4,14111*
Pt-PVP-TP-COF[18]	8420	0.4 (475nm)	PVP-Pt (6 wt%) 0.054M AA λ>420 nm	*Angew.Chem.Int. Ed. **2019**,58,*

			5.5 °C	*18290.*
TpDTz COF[19]	941	0.2 (400nm)	NiME(10 wt%) TEOA(10 vol %) AM 1.5 --*	*J.Am.Chem. Soc.* ***2019****,141,11082.*
g-$C_{52}N_6$-COF[20]	2518.9	----*	Pt (3 wt%) TEOA(10 vol %) λ>420 nm 12 °C	*Angew.Chem. Int. Ed.* ***2020****, 59, 23845.*
g-$C_{40}N_3$-COF[21]	4120	4.84 (420nm)	Pt (3 wt%) TEOA(10 vol %) λ>420 nm 12 °C	*Nat. Commun.* ***2019****, 10, 2467.*
BpCo-COF-1[22]	59.4	0.46 (420nm)	Pt (0.4 wt%) TEOA λ>420 nm --*	*Appl. Catal.,B* ***2020****, 262, 118271.*

*Note: ----=No description of AQE.

--= No mention of reaction temperature.

References:

1. M. J. F. Revision A.03, G. W. Trucks, H. B. Schlegel, G. E. Scuseria, M. A. Robb, J. R. Cheeseman, G. Scalmani, V. Barone, G. A. Petersson, H. Nakatsuji, X. Li, M. Caricato, A. V. Marenich, J. Bloino, B. G. Janesko, R. Gomperts, B. Mennucci, H. P. Hratchian, J. V. Ortiz, A. F. Izmaylov, J. L. Sonnenberg, D. Williams-Young, F. Ding, F. Lipparini, F. Egidi, J. Goings, B. Peng, A. Petrone, T. Henderson, D. Ranasinghe, V. G. Zakrzewski, J. Gao, N. Rega, G. Zheng, W. Liang, M. Hada, M. Ehara, K. Toyota, R. Fukuda, J. Hasegawa, M. Ishida, T. Nakajima, Y. Honda, O. Kitao, H. Nakai, T. Vreven, K. Throssell, J. A. Montgomery, Jr., J. E. Peralta, F. Ogliaro, M. J. Bearpark, J. J. Heyd, E. N. Brothers, K. N. Kudin, V. N. Staroverov, T. A. Keith, R. Kobayashi, J. Normand, K. Raghavachari, A. P. Rendell, J. C. Burant, S. S. Iyengar, J. Tomasi, M. Cossi, J. M. Millam, M. Klene, C. Adamo, R. Cammi, J. W. Ochterski, R. L. Martin, K. Morokuma, O. Farkas, J. B. Foresman, and D. J. Fox, Gaussian 16, Revision A.03.Gaussian, Inc., 2016, Wallingford CT.
2. J. P. Perdew, K. Burke and M. Ernzerhof, *Phys. Rev. Lett.*, 1996, **77**, 3865-3868.
3. J. P. Perdew, K. Burke and M. Ernzerhof, *Phys. Rev. Lett.*, 1997, **78**, 1396-1396.
4. S. Grimme, S. Ehrlich and L. Goerigk, *J. Comput. Chem.*, 2011, **32**, 1456-1465.
5. W. J. Hehre, R. Ditchfield and J. A. Pople, *J. Chem. Phys.*, 1972, **56**, 2257-2261.
6. P. C. Hariharan and J. A. Pople, *Theor. Chim. Acta*, 1973, **28**, 213-222.
7. J. Bi, W. Fang, L. Li, J. Wang, S. Liang, Y. He, M. Liu and L. Wu, *Macromol. Rapid Commun.*, 2015, **36**, 1799-1805.
8. J. Wirth, R. Neumann, M. Antonietti and P. Saalfrank, *PCCP*, 2014, **16**, 15917-15926.
9. Z. Zhao, Y. Zheng, C. Wang, S. Zhang, J. Song, Y. Li, S. Ma, P. Cheng, Z.

Zhang and Y. Chen, *ACS Catal.*, 2021, **11**, 2098-2107.

10. J. Rossmeisl, A. Logadottir and J. K. Nørskov, *Chem. Phys.*, 2005, **319**, 178-184.
11. E. Jin, Z. Lan, Q. Jiang, K. Geng, G. Li, X. Wang and D. Jiang, *Chem*, 2019, **5**, 1632-1647.
12. W. Li, X. Huang, T. Zeng, Y. A. Liu, W. Hu, H. Yang, Y.-B. Zhang and K. Wen, *Angew. Chem. Int. Ed.*, 2021, **60**, 1869-1874.
13. Y. Wang, W. Hao, H. Liu, R. Chen, Q. Pan, Z. Li and Y. Zhao, *Nat. Commun.*, 2022, **13**, 100.
14. C. Lin, X. Liu, B. Yu, C. Han, L. Gong, C. Wang, Y. Gao, Y. Bian and J. Jiang, *ACS Appl. Mater. Interfaces*, 2021, **13**, 27041-27048.
15. S. Ghosh, A. Nakada, M. A. Springer, T. Kawaguchi, K. Suzuki, H. Kaji, I. Baburin, A. Kuc, T. Heine, H. Suzuki, R. Abe and S. Seki, *J. Am. Chem. Soc.*, 2020, **142**, 9752-9762.
16. R. Lu, C. Liu, Y. Chen, L. Tan, G. Yuan, P. Wang, C. Wang and H. Yan, *J. Photochem. Photobiol., A*, 2021, **421**, 113546.
17. C. Mao, Y. Hu, C. Yang, C. Qin, G. Dong, Y. Zhou and Y. Zhang, *ACS Appl. Energy Mater.*, 2021, **4**, 14111-14120.
18. J. Ming, A. Liu, J. Zhao, P. Zhang, H. Huang, H. Lin, Z. Xu, X. Zhang, X. Wang, J. Hofkens, M. B. J. Roeffaers and J. Long, *Angew. Chem. Int. Ed.*, 2019, **58**, 18290-18294.
19. B. P. Biswal, H. A. Vignolo-González, T. Banerjee, L. Grunenberg, G. Savasci, K. Gottschling, J. Nuss, C. Ochsenfeld and B. V. Lotsch, *J. Am. Chem. Soc.*, 2019, **141**, 11082-11092.
20. J. S. Xu, C. Yang, S. Bi, W. Y. Wang, Y. F. He, D. Q. Wu, Q. F. Liang, X. C. Wang and F. Zhang, *Angew. Chem. Int. Edit.*, 2020, **59**, 23845-23853.
21. M. Wang, M. Ballabio, M. Wang, H. H. Lin, B. P. Biswal, X. Han, S. Paasch, E. Brunner, P. Liu, M. Chen, M. Bonn, T. Heine, S. Zhou, E. Canovas, R. Dong and X. Feng, *J. Am. Chem. Soc.*, 2019, **141**, 16810-16816.

22. J. Chen, X. P. Tao, C. Z. Li, Y. H. Ma, L. Tao, D. Y. Zheng, J. F. Zhu, H. Li, R. G. Li and Q. H. Yang, *Appl. Catal. B-Environ*, 2020, **262**, 118271.